#### **TECHNICAL PAPER**



# Tube drawing analysis using upper bound and energy methods and validation by Cockcroft-Latham failure criteria

Vahid Pouyafar<sup>1</sup> · Hadi Bolandi<sup>1</sup> · Ramin Meshkabadi<sup>2</sup>

Received: 22 June 2021 / Accepted: 22 November 2021
© The Author(s), under exclusive licence to The Brazilian Society of Mechanical Sciences and Engineering 2021

#### Abstract

Cold tube drawing reduces the tube dimensions with closed tolerances and improves its mechanical properties. In this paper, there was an investigation into the cold drawing process with a floating plug using an upper bound analysis and energy method. The ring compression test was performed to determine the friction coefficient. Grooved pipe testing was done to determine the critical damage value. Simulation results confirmed the values of 0.05 for friction coefficient and 0.862 for critical damage value. Using the design of experiments with Taguchi method, the upper bound analysis was done and the correct design parameters were selected. For the selected parameters, the stress value of 289 MPa was obtained from the upper bound analysis. The design process was simulated using ABAQUS software and the results of the stress analysis at the die output showed the consistency of the upper bound analysis and simulation results.

Keywords Tube drawing · Floating plug · Finite element method · Taguchi method · Cockcroft-Latham failure criteria

## 1 Introduction

Tubular materials are applied in different industries such as aerospace, defense, nuclear, and transportation [1–3]. The cold tube drawing is used to reduce the close tolerance, and increase surface quality to achieve better mechanical properties [4, 5]. This process is divided into four drawing classes: without the plug (hollow sinking), with a mandrel, and with a fixed and floating plugs [6].

Process design and optimization through experimental analysis require costly trial-and-error methods. Therefore, theoretical analysis and process design to reach the optimized conditions are crucial before the manufacturing and industrial development. There are various methods to analyze the tube drawing: analysis of plug position in the deformation zone [7], differential equilibrium equations [8], residual stresses

Technical Editor: Lincoln Cardoso Brandao.

□ Vahid Pouyafar pouyafar@tabrizu.ac.ir

Published online: 08 December 2021

- Manufacturing Engineering Department, University of Tabriz, Tabriz, Iran
- Department of Engineering Sciences, Faculty of Advanced Technologies, University of Mohaghegh Ardabili, Namin, Iran

[9], and energy methods [10]. Analyzing the plug position at the deformation zone assumes the plug position at the possible extreme foremost or the extreme rearmost as shown in Fig. 1. If the plug is in the extreme foremost position, the tube thickness remains constant at the deformation zone. In addition, it is possible to assume the plug in the rearmost position, resulting in a reduction of friction between the tube and the plug. Rubio [10] showed that these two states do not exist in practice and proved that the actual plug position is between these two positions.

Classical methods of analysis including homogenous deformation and slab analysis estimate the amount of required energy to perform the process less than the actual amount. The first one assumes the required energy for a homogenous deformation and the second one assumes the required energy to dominate friction rather than the homogenous deformation. Upper bound analysis allows evaluating the term due to the internal distortion that suffers the material when it is being deformed [12]. Kwan [13] proposed the upper bound method and calculated internal distortion during deformation caused by the so-called redundant energy.

The success of the metal forming process is mainly predicted by ductile failure. A ductile failure is one where there is substantial distortion or plastic deformation of the failed part. Normally, a component will fail in a ductile manner when it plastically deforms, and the steadily reducing cross section



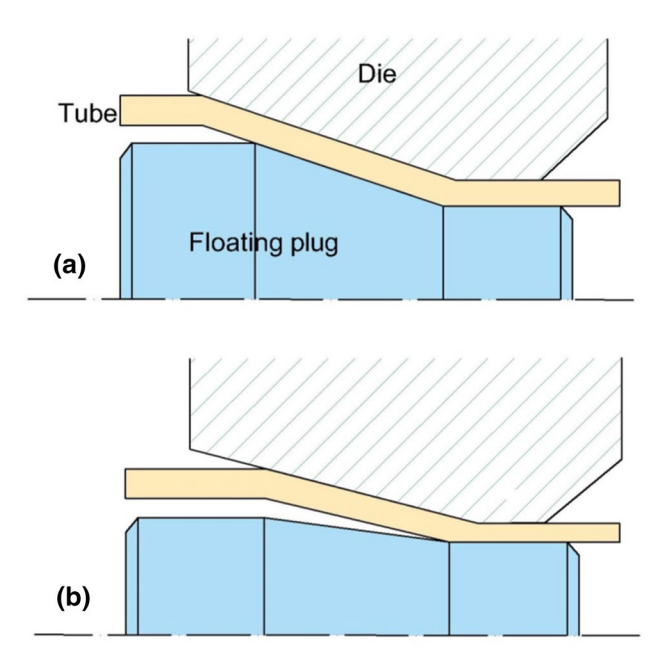


Fig. 1 a Extreme foremost and  $\mathbf{b}$  extreme rearmost plug positions [11]

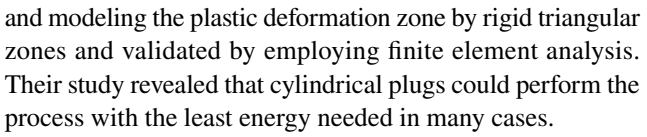
can no longer carry the applied service load. If it is possible to predict the deformation conditions that will lead to failure, it will be possible to select the right process conditions and optimize the forming process to produce safe products. The ductile failure criterion is based on the experimental works. The Cockcroft-Latham criterion is based on the theory of cumulative damage, which has been used successfully for a variety of loading conditions. It has the advantage of the experimental approach and mathematical computation. It is expressed as:

$$C = \int_{0}^{\overline{\epsilon}f} \left(\frac{\sigma_T}{\overline{\sigma}}\right) d\overline{\epsilon}$$
 (1)

where  $\sigma_T$  is the maximum tensile stress,  $\overline{\sigma}$  the effective stress,  $d\overline{\epsilon}$  the increment of effective strain,  $\overline{\epsilon}_f$  the sum of the equivalent strains is at the end of the forming process, and C is a constant value for a given material. To prevent failure, the C value should not exceed the critical damage value [14, 15].

Świątkowski and Hatalak [11] used the actual plug position and diameter by investigating the drum-drawing process with a floating plug in thin-walled tubes. This approach led to the development of a new tool for geometry design. It minimized the tube-sinking zone, increased the wall-thickness reduction, and stabilized the process.

Recently, Rubio and Camacho [16] proposed some practical guidelines to select a set of plugs to perform the drawing process of thin-walled tubes. They considered the tube material, geometrical parameters, and the friction conditions. They analyzed the process through the upper bound method



Rubio [10] has studied the drawing process with a fixed plug by an upper bound method of energy. The inner diameter was constant along the process for simplifying the energy equation. They studied the effects of cross-section area reduction, die conical semi-angle, and fixed plug. They obtained the optimum conditions of the minimum energy consumption. Kwan [13] proposed an arbitrary four-order polynomial curve for die and plug and calculated the admissible velocity field through differentiating curve functions. He conducted the upper bound analysis according to the boundary conditions and flow characteristics of symmetric drawing.

Kuboki, Nishida [17] designed a tube drawing process with a fixed tapered plug. They conducted the upper bound analysis to investigate the various parameters' effects. There was an investigation of the plug's existence and the area reduction on the residual stress in a tube drawing process. They showed that the plug's existence causes a more homogenous stress distribution along with increased tensile loads.

Lee, Ko [15] suggested a drawing process for a steering input shaft by defining a criterion for the critical damage value. They evaluated the critical damage value by a compression test for two types of arc and conical profiles. The results showed that the arc profile had a higher damage value because of the sudden deformation compared to the conical one. Haddi, Imad [18] investigated the influence of drawing conditions on temperature rise and drawing stress in cold-drawn copper wires using experimental methods. They showed that the drawing stress and temperature rise vary during the drawing process because of the friction coefficient and the flow stress.

Toribio et al. [19] analyzed the influence on hydrogen embrittlement of the inlet die angle and the die bearing length through the finite element method (FEM). They concluded that the effects of residual stress and strain fields produced by wire drawing on hydrogen embrittlement were less dangerous when the inlet die angle decreased or when the bearing length exceeded the wire radius.

Chobaut, Drezet [20] determined the friction coefficient and drawing limit of 316 LVM stainless steel in the tube drawing with a fixed plug. They compared the measured and simulated drawing forces and determined the friction coefficients between tube and die and tube and plug. Cao [21] reviewed the fracture prediction models to obtain actual results for both geometry precision and mechanical properties.

Kong et al. [22] investigated the effect of mechanical property on the forming limit of DP780 specimens. They predicted the forming limit based on the experiments and the finite element analysis and compared it with the Cockcroft-Latham ductile fracture criterion. Farahani et al. [23] dealt with presenting an optimum curved die profile in the tube



drawing process with a fixed conical plug. They investigated the drawing stress based on incremental slab method theory and determined the optimum die profile. They demonstrated that the required tension stress in the tube drawing process with an optimum die profile decreased compared to the same process with a conical die profile.

Until now, previous studies utilized the process design methods separately. It is evident that a successful design must consider different parameters, which require the different analysis methods cooperatively. However, there is no study in the literature, which deals with the design problem in this way. Thus, the authors studied the tube drawing process with a floating plug by a combination of the upper bound and energy methods. The plug position and the diameter at the deformation zone were investigated. The design has been simulated and verified through a finite element analysis.

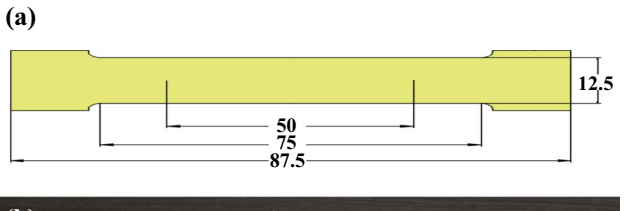
#### 2 Materials and methods

# 2.1 Material properties and dimensions

St 37 steel tube with an outer diameter of 21.3 mm and a wall thickness of 2.77 mm was used as a raw material according to ASTM A53 [24]. The elastic modulus and the Poisson's ratio are 207 GPa and 0.3, respectively.

### 2.2 Tensile test

The mechanical properties of the material, including yield stress, ultimate strength, and stress-strain equation were obtained via the standard tensile test at an ambient temperature. Two test specimens (Fig. 2a) were prepared through a



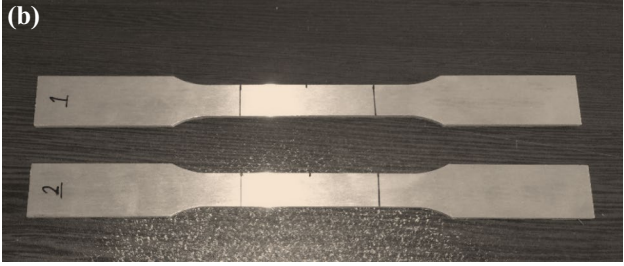


Fig. 2 a First test sample dimensions [25] and **b** prepared samples for tensile test

wire cut from a plate of 3 mm thickness and were ground to 2.7 mm before the test, as shown in Fig. 2b. The tensile test was conducted using the ASTM E8 M standard by the Shimadzu universal testing machine AG-25 TB model [25]. The obtained mechanical properties and the stress–strain equation through the tensile test are presented in Table 1. Figure 3a shows the specimens after the tensile test, and Fig. 3b presents the true stress–strain curve and its comparison with the curve obtained from the developed model.

## 2.3 Ring compression test

The ring compression test was performed to determine the friction coefficient. The material used for dies was D2 tool steel hardened to 61RC. The outer diameter, inner diameter, and height of the specimens were 30, 15, and 10 mm, respectively. The specimens were pressurized in a universal testing machine with a capacity of 80 tons, and their dimensional changes were measured. Each test was repeated three times to ensure the results. Figure 4 shows the samples before and after the test. To determine the friction coefficient, the ring compression test was simulated with different friction coefficients (0.01, 0.02, 0.03, 0.04, 0.05, 0.06, and 0.07)

**Table 1** Mechanical properties and stress-strain equation of the material (The values correspond to the engineering stress)

Stress-strain relation	Elongation (%)	Ultimate stress (MPa)	Yield stress (MPa)	
$\sigma = 738\epsilon^{0.234}$	36	415	310	



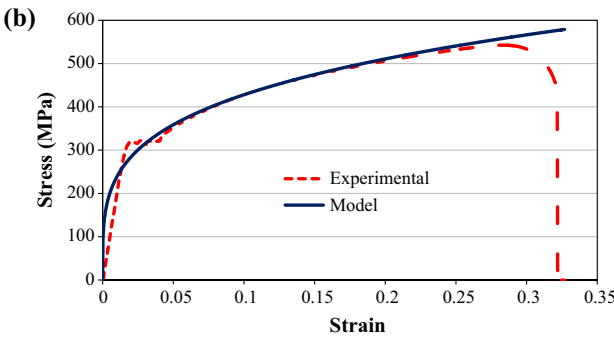


Fig. 3 a Tensile test specimens after the test and b obtained true stress-strain curve and comparison with the developed model



Page 4 of 12

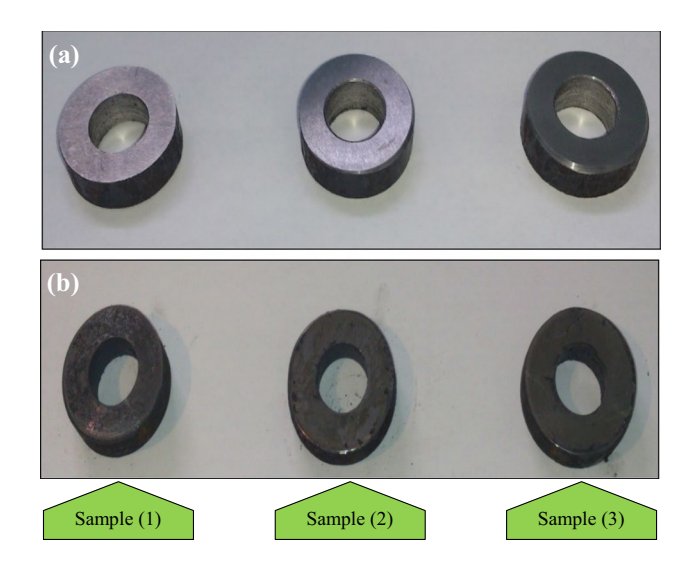
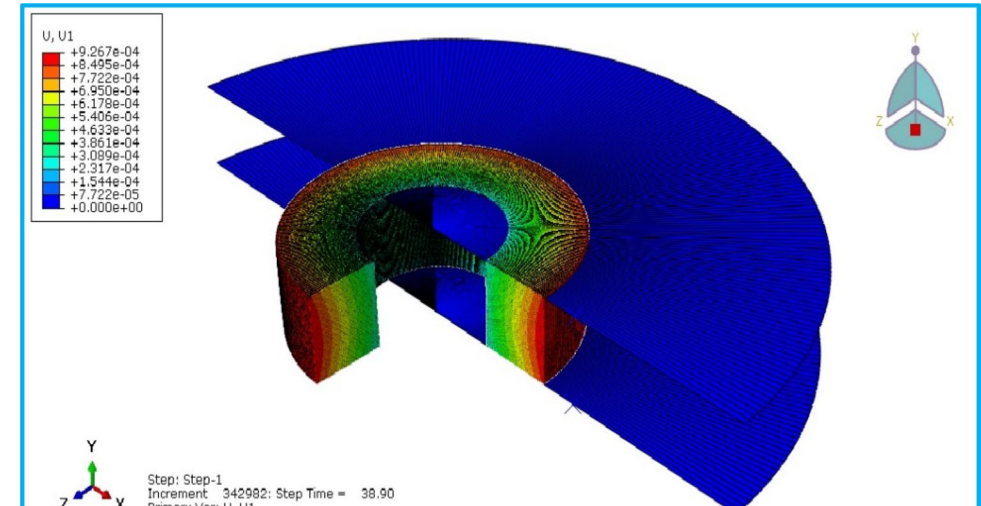


Fig. 4 Samples prepared for ring compression test  $\boldsymbol{a}$  before and  $\boldsymbol{b}$  after the test

in ABAQUS software. The meshing type was CAX4R, as shown in Fig. 5. Table 2 presents the extracted results of the dimensional changes from the practical and simulation tests in different friction coefficients.  $D_{\rm o}$ ,  $D_{\rm i}$ , and h are the outer diameter, inner diameter and height of the specimens, respectively. In conclusion, the simulation result with a friction coefficient of 0.05 is more in line with the results of the practical tests.

## 2.4 Grooved pipe testing

In two previous studies [15, 26], specimens with three different H/D (height/diameter) ratios (1, 1.25, and 1.5) were utilized for this experiment. Their results showed that the H/D ratio does not affect the critical damage value, so the larger ratio of 1.5 is neglected in this study. In this study, pipes with a 1 mm groove along the cylindrical axes and H/D ratios of 1 and 1.25 were used to ensure that the



**Fig. 5** Simulation result of ring compression test

**Table 2** Results of finite element simulation and practical ring compression test

Sample No	Friction	$\Delta D_o$ (r	nm)	Error (%)	$\Delta D_i$ (n	nm)	Error (%)	Δh (mm)
coet	coefficient	Exp	Sim		Exp	Sim		
1	0.01	1.84	1.972	7.2	0.58	0.918	58	-1.22
1	0.02	1.84	1.942	5.5	0.58	0.834	44	-1.22
1	0.03	1.84	1.912	3.9	0.58	0.75	29	-1.22
1	0.04	1.84	1.882	3.2	0.58	0.664	14	-1.22
1	0.05	1.84	1.852	0.6	0.58	0.578	3.5	-1.22
1	0.06	1.84	1.822	1	0.58	0.454	21	-1.22
2	0.04	2.03	2.056	1.3	0.64	0.684	7	-1.32
2	0.05	2.03	2.02	0.5	0.64	0.624	2.5	-1.32
2	0.06	2.03	1.982	2	0.64	0.494	23	-1.32
3	0.04	1.94	1.982	2.2	0.61	0.656	7.5	-1.27
3	0.05	1.94	1.934	0.3	0.61	0.602	1.3	-1.27
3	0.06	1.94	1.904	1.9	0.61	0.476	22	-1.27



critical damage value is not affected by the sample geometry. The outer and inner diameters of the specimens were 21.3 and 15.8 mm. The specimens were pressurized with a 25-ton press and were ground to apply the axial pressure, perpendicular to the specimen's cross-section. When the cracks appeared in the grooves, the pressure is stopped. Figure 6 shows the grooved pipes and sample location in the testing machine.

The finite element software (ABAQUS) was used to simulate the tests and obtain the critical damage value. The critical damage values were calculated using the integral formula of Cockcroft-Latham criterion. Figure 7 shows the

simulation results and the tested samples. Table 3 presents the crack height and the critical damage. As mentioned before, the critical damage values have not changed and equal to 0.862.

## 2.5 Die and plug design

The b-spline curve with four controlling points was used for the die profile. According to Lee et al., conic profiles are better than the arc ones for the dies [15]. It is due to the abrupt deformation at the inner part of the arc-shaped dies.

**Fig. 6** Prepared grooved tubes and sample placement in the testing machine

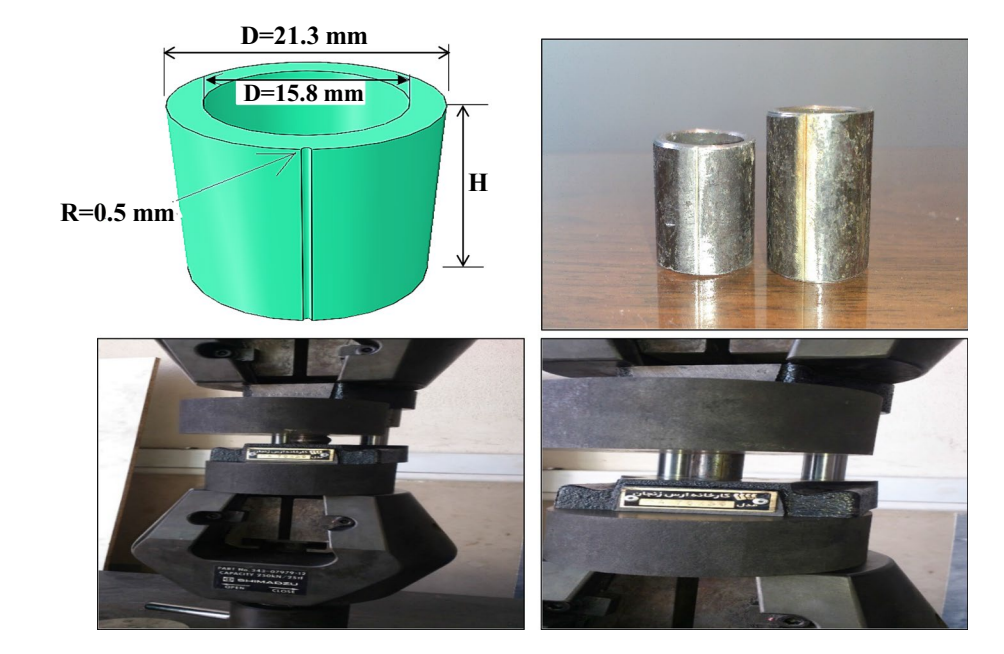


**Fig. 7** Actual and simulated samples after compression test with H/D ratio of (a) 1 and (b) 1.25

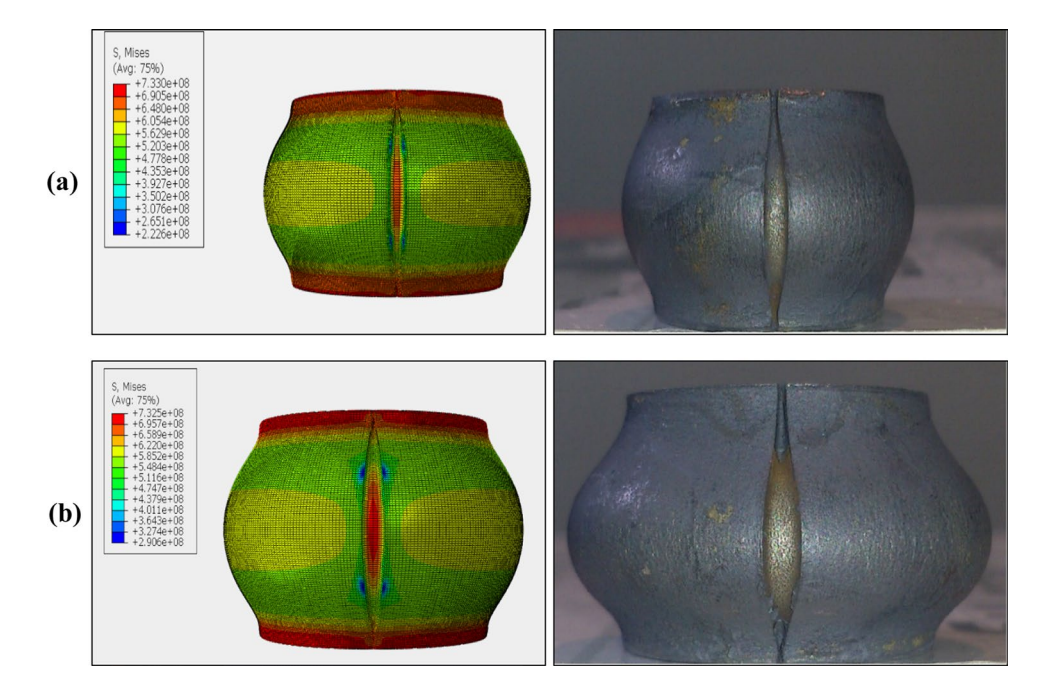




**Table 3** Crack height and the critical damage value for grooved tube testing

H/D ratio	Sample number	Crack height (mm)	Critical damage value
1	A	13.75	0.876
1	В	13.84	0.881
1.25	C	16.59	0.862
1.25	D	16.27	0.898

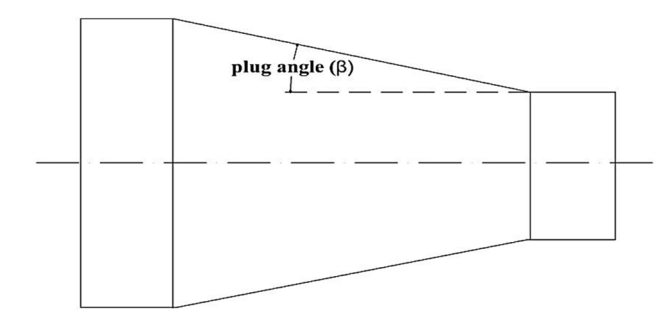


Fig. 8 Schematic of floating plug with  $\beta$  semi-angle

Therefore, the degree of b-spline was set to one. The polygon consists of segments crossing all of the control points. The obtained equations of the die are as follows:

$$P(u) = \begin{cases} P_0(1-u) + P_1 & 0 \le u \le 1 \\ P_1(2-u) + P_2(u-1) & 1 \le u \le 2 \\ P_2(3-u) + P_3(u-2) & 2 \le u \le 3 \end{cases} \tag{2}$$

where P(u) is the b-spline curve,  $P_0$ ,  $P_1$ ,  $P_2$ , and  $P_3$  are controlling points, and u is the independent variable. Figure 8 shows the conic profile of the floating plug with the  $\beta$  semi-angle. The diameter of the small cylindrical area equals the inner diameter of the tube when leaving the mold. The

diameter of the large cylindrical area is between the plug's working diameter and the tube's inner diameter at the inlet.

Figure 9 shows the deformation region in the tube drawing process with a floating plug schematically.

The researcher used the developed equations by Swiat-kowski and Hatalak [11, 27] to obtain the plug back-track  $(n_r)$  and real diameter  $(d_r)$  according to Eqs. (3) and (4). It is assumed that the applied pressure to different plug parts is uniform

$$d_r = \sqrt{\left(d_k + R\frac{\sin{(\alpha + \omega - \beta)}}{\sin{(\alpha + \omega)}}\right)^2 + 4R\left(l_d + n_{\max}\right)\sin{\beta}} - R\frac{\sin{(\alpha + \omega - \beta)}}{\sin{(\alpha + \omega)}}$$
(3)

$$n_r = n_{\text{max}} \frac{\left(d_r - d_k\right) \sin\left(\alpha + \omega - \beta\right)}{2 \sin\left(\alpha + \omega\right) \sin\beta} \tag{4}$$

As shown in Fig. 9,  $d_k$ ,  $\alpha$ ,  $\beta$ , and  $l_d$  are tube internal diameter in the output, die semi-angle, plug semi-angle, and the cylindrical die length, respectively. R,  $\omega$ , and  $n_{max}$  were calculated as [11, 27]:

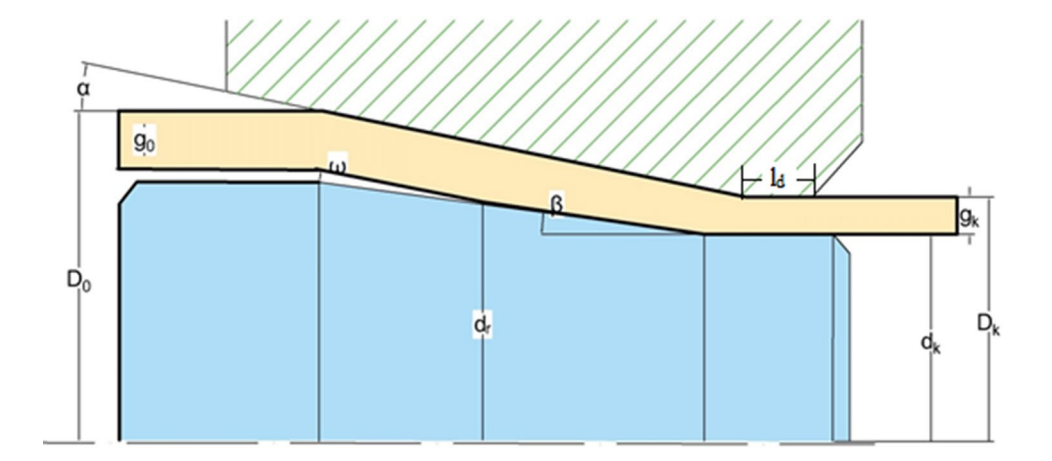
$$R = \frac{\mu d_k}{(\sin \beta - \mu \cos \beta)} \tag{5}$$

$$\omega = \arctan \frac{2\Delta g \sin \alpha}{2g_0 \cos \alpha + d_0 - d_k - 2g_0} \tag{6}$$

$$n_{\text{max}} = g_k \tan \alpha + \frac{\left(g_0 + \Delta g - \left(\frac{g_k}{\cos \alpha}\right)\right) \cos \omega}{\sin (\alpha + \omega)}$$
 (7)

Here,  $\mu$ ,  $g_0$ ,  $g_k$ ,  $d_0$ , and  $d_k$  are friction coefficient, the tube initial thickness, the tube thickness at the outlet, and the tube external diameter at the inlet and outlet of the die, respectively.  $\Delta g$  is the difference between the tube outlet and inlet thicknesses.

Fig. 9 Schematic of tube drawing process with floating plug [11]





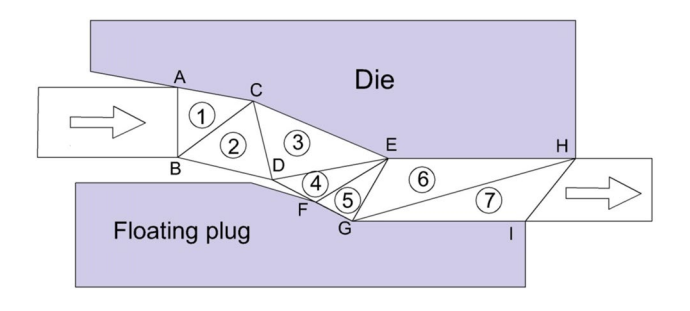


Fig. 10 Schematic of the deformation zone modeled by triangular rigid zones

# 2.6 Upper bound analysis

For the upper bound analysis, the deformation region is divided into the rigid triangular zones corresponding to the deformation region geometry according to Fig. 10. Figure 11 shows the hodograph of the shear zones. By assuming no strain-hardening in the material and by equalizing the rate of consumed internal and external energies, the force value greater than the actual force is calculated [27].

# 2.7 Applying the energy method

By analyzing the hodograph of each shear zone and equating the internal energy consumption rate with the external forces, we will have:

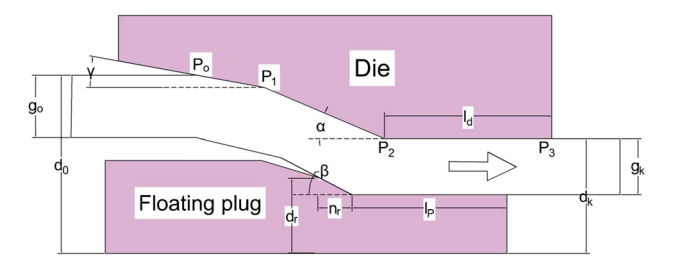


Fig. 12 Schematic of the deformation zone with marked design parameters and controlling points

Table 4 Design parameters

Conical semi-angle of the plug	Cylindrical length of the plug	2	Secondary semi-angle of die	Inlet semi- angle of die
β	$l_p$	l <sub>d</sub>	α	Υ

Here,  $\sigma_{xf}$ ,  $d_k$ ,  $g_k$ , and  $V_f$  are the stress, diameter, thickness, and velocity of the tube in the output of the die, respectively. k is the shear yield stress, and  $\mu$  is the friction coefficient at the surface.  $kV_{AB}^* \overline{AB}$ ,  $kV_{BC}^* \overline{BC}$ ,  $kV_{CD}^* \overline{CD}$ ,  $kV_{DE}^* \overline{DE}$ ,  $kV_{EF}^* \overline{EF}$  and  $kV_{EG}^* \overline{EG}$  phrases are the mechanical effects along the  $\overline{AB}$ ,  $\overline{BC}$ ,  $\overline{CD}$ ,  $\overline{DE}$ ,  $\overline{EF}$ , and  $\overline{EG}$ , respectively.  $\mu PV_{AC}^* \overline{AC}$ ,  $\mu PV_{CE}^* \overline{CE}$ , and  $\mu PV_{EH}^* \overline{EH}$  are friction effects between the material and the die along the  $\overline{AC}$ ,  $\overline{CE}$ , and  $\overline{EH}$ . On the other side,  $\mu PV_{FG}^* \overline{FG}$  and  $\mu PV_{GI}^* \overline{GI}$  are friction effects between the

$$\frac{\mathrm{d}W}{\mathrm{dt}} = \sigma_{xf}\pi d_k g_k V_f = 2\pi d_k \left( kV_{AB}^* \overline{AB} + kV_{BC}^* \overline{BC} + kV_{CD}^* \overline{CD} + kV_{DE}^* \overline{DE} + kV_{EF}^* \overline{EF} + kV_{EG}^* \overline{EG} + \mu PV_{AC}^* \overline{AC} \right) \\
+ \mu PV_{CE}^* \overline{CE} + \mu PV_{EH}^* \overline{EH} + \mu PV_{FG}^* \overline{FG} + \mu PV_{GI}^* \overline{GI} \right)$$
(8)

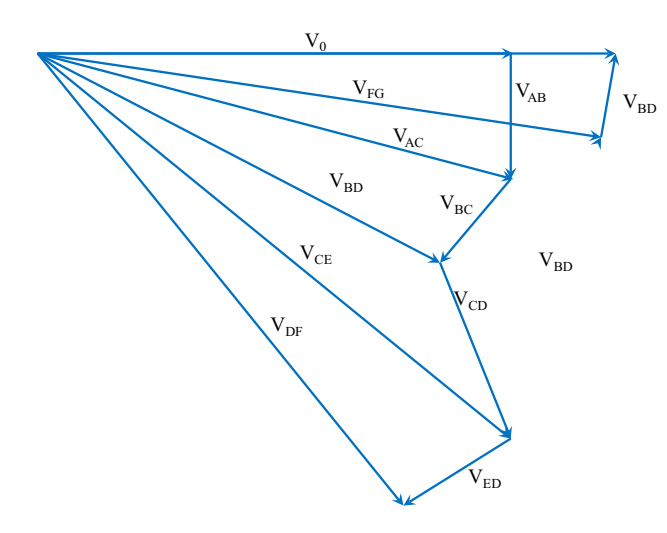


Fig. 11 The hodograph

tube and the floating plug along  $\overline{FG}$  and  $\overline{GI}$ . Assuming the equal pressure P at the die and the plug, principal stresses are equal to  $\sigma_1 = \sigma_x$  and  $\sigma_2 = -P$  so that according to the yield plane strain condition, we will have:

$$P + \sigma_{xf} = 2k \to P = 2k - \sigma_{xf} \tag{9}$$

Table 5 Geometric dimensions and required properties in the upper bound method

Parameter	Symbol	Value
The inlet thickness of tube (mm)	$g_0$	2.77
The output thickness of tube (mm)	$g_k$	2.57
The inlet external diameter of tube (mm)	$d_o$	21.3
The outlet external diameter of tube (mm)	$d_k$	18
Friction coefficient	μ	0.05
Shear yield stress (MPa)	k	155
The outlet velocity of tube (m/min)	$V_{\rm f}$	1



Page 8 of 12

By placing Eq. (7) into Eq. (6), the magnitude of  $\sigma_x$  was

(10)

was used in the MINITAB software. Table 7 shows the designed experiments according to the L<sub>0</sub> orthogonal array.

$$\sigma_{xf} = 2k \left[ \frac{V_{AB}^* \overline{AB} + V_{BC}^* \overline{BC} + V_{CD}^* \overline{CD} + V_{DE}^* \overline{DE} + V_{EF}^* \overline{EF} + V_{EG}^* \overline{EG}}{g_k V_f + 2\mu \left(V_{AC}^* \overline{AC} + V_{CE}^* \overline{CE} + V_{EH}^* \overline{EH} + V_{FG}^* \overline{FG} + V_{GI}^* \overline{GI}\right)} + \frac{2\mu \left(V_{AC}^* \overline{AC} + V_{CE}^* \overline{CE} + V_{EH}^* \overline{EH} + V_{FG}^* \overline{FG} + V_{GI}^* \overline{GI}\right)}{g_k V_f + 2\mu \left(V_{AC}^* \overline{AC} + V_{CE}^* \overline{CE} + V_{EH}^* \overline{EH} + V_{FG}^* \overline{FG} + V_{GI}^* \overline{GI}\right)} \right]$$

# 2.8 Design of experiments for process design optimization

Based on the calculations made in Sect. 2.5., and as shown in Fig. 12, the design parameters can be considered according to Table 4.

The geometric parameters and the required mechanical properties in the upper bound analysis are according to Table 5.

Table 6 shows the efficient design parameters and the appropriate levels of them. Based on the mentioned calculations and the previous research by Światkowski and Hatalak [11], the optimal value of  $\alpha$ - $\beta$  is within the range of 2 to 3°. Therefore, the angular parameter  $\beta$  depends on the angle  $\alpha$ and is an independent parameter.

Due to the number of factors and levels of experiments, it is necessary to perform 81 tests. To reduce the experiment's time and cost, the design of experiments (Taguchi method)

Table 6 Design parameters and related levels

Parameter	Leve	1	
	1	2	3
γ (°)	5	7.5	10
α (°)	10	15	20
$l_{d}$ (mm)	10	12	14
$l_p (mm)$	6	8	10

Table 7 L<sub>9</sub> orthogonal array for drawing die optimization design

Experiment No	γ (°)	α (°)	l <sub>d</sub> (mm)	l <sub>p</sub> (mm)
1	5	10	10	6
2	7.5	10	12	10
3	10	10	14	8
4	5	15	12	8
5	7.5	15	14	6
6	10	15	10	10
7	5	20	14	10
8	7.5	20	10	8
9	10	20	12	6

Table 8 Stresses at the die exit calculated by the upper bound analysis

Experiment No	1	2	3	4	5	6	7	8	9
Drawing stress (MPa)	340	334	384	330	315	337	370	298.5	342



#### 2.9 Process simulation

The process simulation was carried out using the ABAQUS software to validate the upper bound analysis. The simulation is performed as an axial symmetry. The tube was deformable, and the die and plug were rigid. The simulation was performed with a dynamic/explicit code. The time increments were calculated by the ABAQUS automatically. The contact properties were assumed as Coulomb friction with friction coefficient of 0.05. To justify the fact that the two contacts (die/tube and plug/tube) are similar in the process simulation, the die and plug were made from D2 tool steel with the same hardness and roughness. For boundary conditions, the die was fixed, the plug was free to move, and the tube was drawn into the die. The meshing of the tube was CAX4R. It is a 4-node, reduced-integration, first-order, axisymmetric solid element. Approximate element size was 0.02 to 0.05 mm.

#### 3 Results and discussion

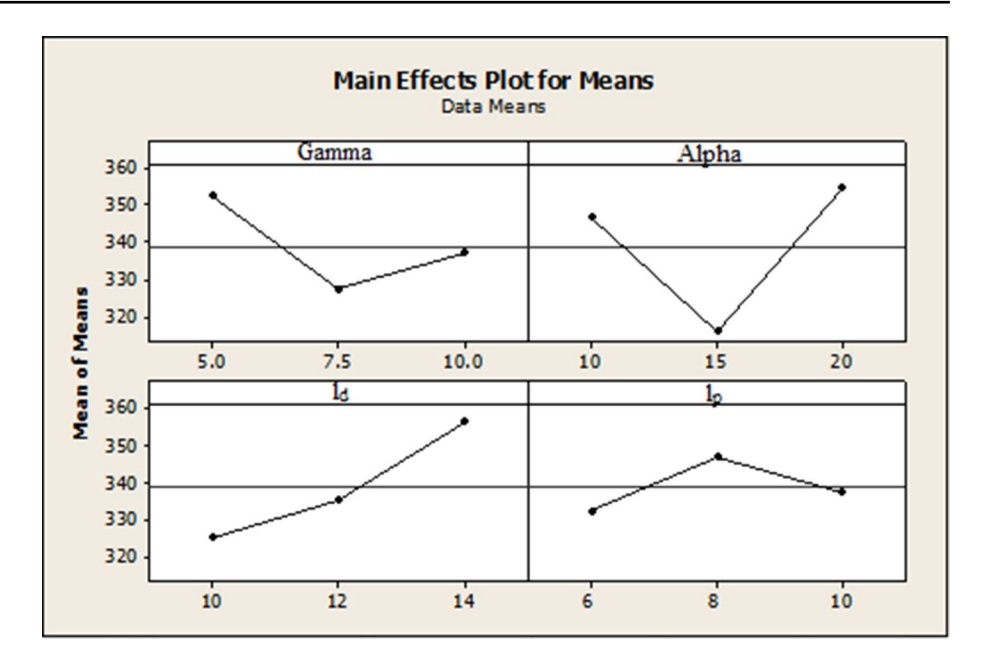
# 3.1 Upper bound analysis results and effects of design parameters

Table 8 lists the calculated drawing stresses from the upper bound analysis. Figures 13 and 14 show the mean of S/N ratio and the mean of means diagrams on the drawing stresses obtained by the upper bound analysis. The responses are extracted based on the "smaller is better" criterion.

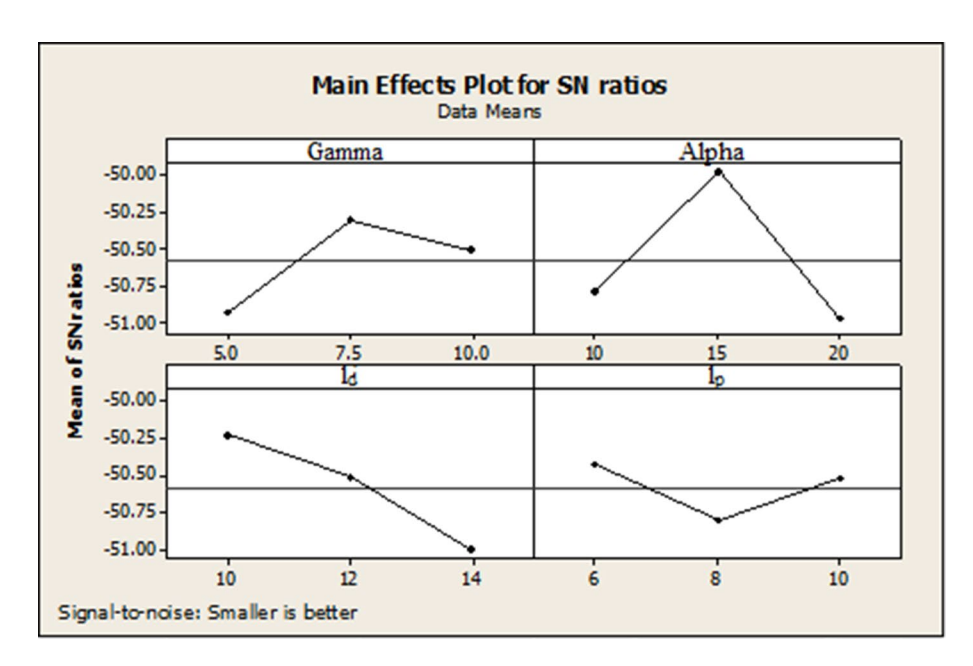
According to Figs. 13 and 14, the angles of  $\gamma$  and  $\alpha$ , at 7.5° and 15°, the die cylinder length (l<sub>d</sub>) at 6 mm and the plug cylinder length (l<sub>p</sub>) at 10 mm are the most optimal conditions for the design parameters. The drawing stress from the upper bound analysis for the optimal case was 289 MPa. Equation 9 can be used to find the contribution of each of the investigated design parameters (PA) on the amount of drawing stresses.

$$PA = S_A \cdot \frac{100}{S_T} \tag{11}$$

**Fig. 13** Mean of means analysis of drawing strength



**Fig. 14** S/N ratio analysis of drawing strength



$$S_T = \frac{\sum_{i=1}^n Y_i^2 - (\sum_{i=1}^n Y_i)^2}{n}$$
 (12)

$$S_A = \frac{A_1^2}{N_{A1}} + \frac{A_2^2}{N_{A2}} + \dots + \frac{A_m^2}{N_{Am}} - \frac{(\sum_{i=1}^n Y_i)^2}{n}$$
 (13)

where Y is the response of each experiment and n is the experiment number in the Taguchi method.  $A_m$  is the sum of all the responses of the experiments, and  $N_{AM}$  is the number of tests. The percentage contribution was calculated according to the data in Tables 7 and 8. Figure 15 shows the results

as a pie chart. Table 9 presents the final design parameters based on the obtained drawing stress of the optimum design state (289 MPa). Figure 15 shows that the die semi-angle ( $\alpha$ ) with an optimal value of 15 ° has the greatest effect on reducing the drawing stresses calculated by the upper bound method. The cylindrical die length ( $l_d$ ) with an optimal value of 10 mm is in the second place of reducing the created stresses. The inlet semi-angle of die ( $\gamma$ ) with an optimal value of 7.5° is in the third rank of the effective parameters in reducing the stresses. The effect of the cylindrical length of the plug ( $l_p$ ) is less compared to other parameters.



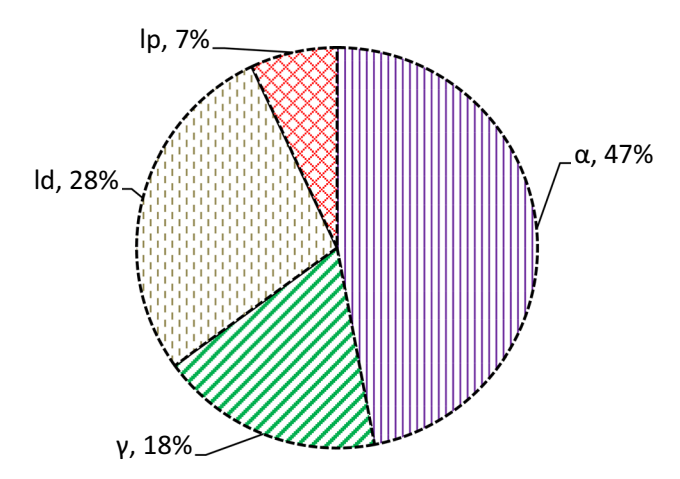


Fig. 15 Percentage contribution of design parameters on response (drawing stress)

Table 9 Final design parameters

Parameter	γ (°)	α (°)	l <sub>d</sub> (mm)	l <sub>p</sub> (mm)	β (°)
Value	7.5	15	10	6	12.7

## 3.2 Simulation of the drawing process

The finite element simulation was conducted in the optimal conditions using the ABAOUS software to validate the upper bound analysis results. The tube was a deformable part, whereas the plug and the die were perfectly rigid. The mechanical properties were determined through the obtained stress-strain relation. Modeling was carried out asymmetrically with dynamic/explicit code. The Coulomb friction state with a friction coefficient of 0.05 was chosen for the contact surfaces. Figure 16 represents the von Mises stress distribution. There are obviously other stresses than the tensile one during forming process. The tensile test is studied here because it is the stress given by the upper bound and energy methods. This model was then used to simulate the drawing process. The drawing stress obtained from the simulation is less than 290 MPa, consistent with the calculated value from the upper bound analysis (Fig. 17). The stress in Fig. 17 is the stress change over time for an inner diameter element of the tube.

## 3.3 The amount of damage in the process

The authors evaluated the design suitability and process failure prediction by employing the Cockcroft-Latham failure criterion. In Sect. 2.4., the critical value of the damage through the experimental tests and simulation was obtained to be 0.862. According to the damage criterion theory mentioned in

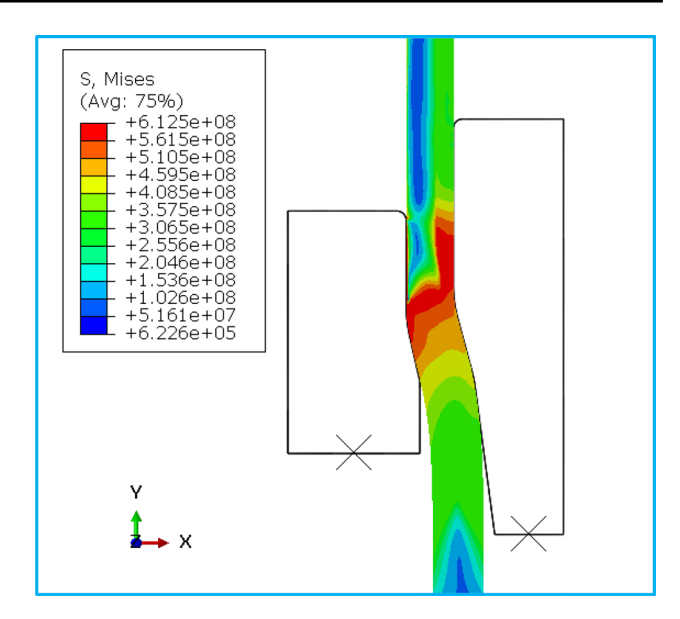


Fig. 16 Stress distribution contour in the tube drawing with floating plug

Introduction section, if the damage value is less than the critical value, the failure does not occur according to the Cockcroft-Latham failure Criteria. If the calculated damage value is more than that value, the failure occurs, and the design must carry out again.

The simulated process in Sect. 3.2 is examined to quantify the damage. The tube damage was calculated using the Cockcroft-Latham failure criteria. The results of the damage value in the tube elements show that this value reaches a maximum of 0.477, which is significantly lower than the critical value of 0.862; therefore, according to the Cockcroft-Latham failure criteria, no failure will occur. According to Fig. 18, investigations show that the damage of tube surfaces in contact with the die and plug is more than the inside, and in the adjacent elements of the plug, it is larger than the adjacent elements of the die. Table 10 represents the calculated damage values for the Taguchi design experiments using the simulation and Cockcroft-Latham failure criteria. It is necessary to mention that the Cockcroft-Latham damage value is a dimensionless positive parameter, which depends on the state of the applied stress. The critical value of this criterion is a characteristic of every material and for the ductile low carbon steels it is around 1.

## 4 Conclusions

In this study, the process of tube drawing design with a floating plug was carried out by an upper bound analysis, an energy method, and an analysis of the floating plug's actual position and diameter.



Fig. 17 Stress changes in the tube drawing process over time for an inner diameter element of the tube

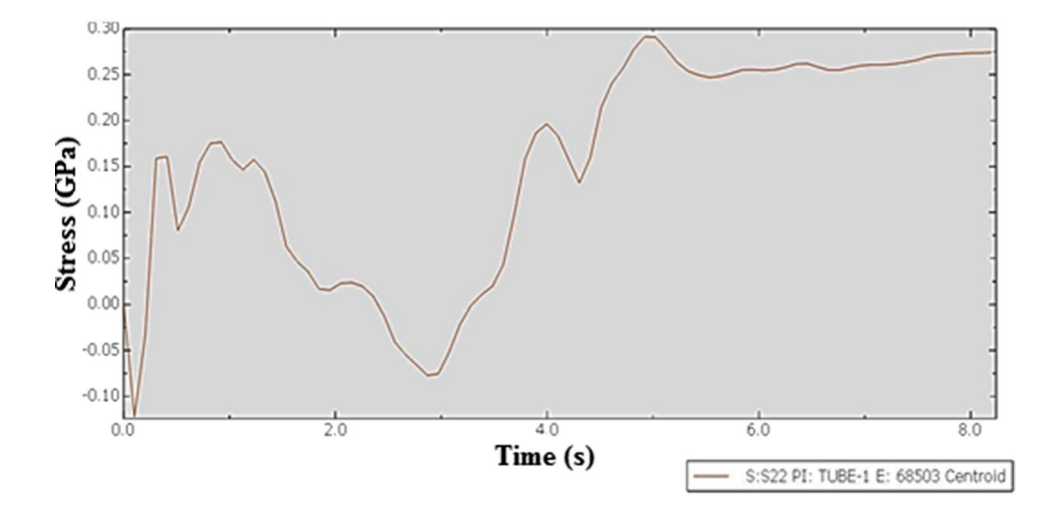
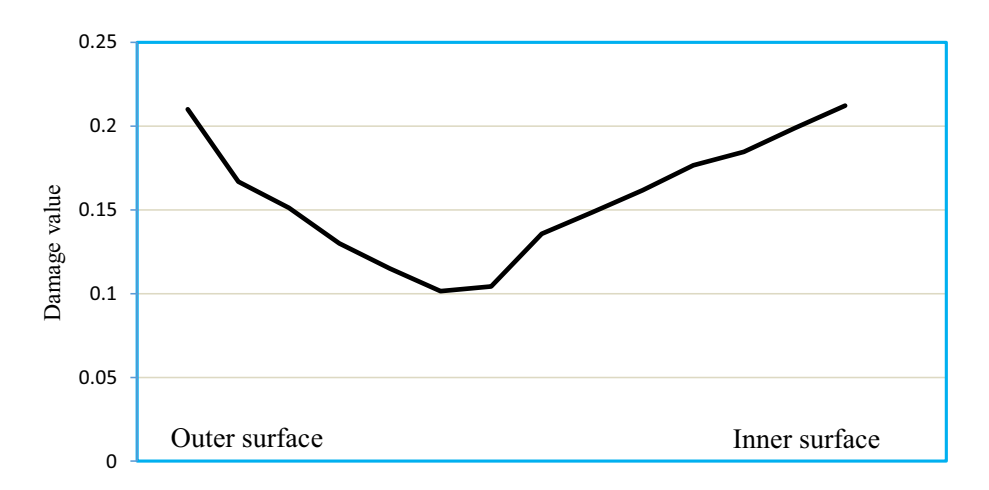


Fig. 18 Changes in the damage value in tube thickness



**Table 10** Critical damage values for designed experiments

Experiment No	1	2	3	4	5	6	7	8	9
Damage value	0.681	0.714	0.837	0.707	0.536	0.694	0.941	0.845	0.921

- The mechanical properties and the stress-strain equations were obtained through the tensile test.
- The ring compression test was performed to determine the friction coefficient. The simulation results were in line with the experimental tests, and the friction coefficient was considered as 0.05.
- The critical damage values were calculated using the integral formula of the Cockcroft-Latham criterion, and it was observed that the critical damage value of different H/D ratios did not change and was 0.862.
- The equation parameters for determining the plug position and actual diameter at the deformation zone were derived through practical experiments of tensile test, ring compression test and grooved pipe test. Then, the upper bound analysis was conducted and the design

- parameters were optimized through the Taguchi method. The drawing stress were extracted based on the "smaller is better" criterion.
- According to the results of the Taguchi method, the angles of γ and α, at 7.5° and 15°, the die cylinder length (l<sub>d</sub>), and the plug cylinder length (l<sub>p</sub>) at 6 and 10 mm were the most optimal conditions, respectively.
- By analyzing the percentage contribution of each parameter on the drawing stress, the parameters α, l<sub>d</sub>, γ, and l<sub>p</sub> had the impacts of 47, 28, 18, and 7%, respectively.
- A finite element simulation was performed to validate the results of upper bound analysis and it was revealed that the simulation results were consistent with the upper bound method. The results showed that the plug position



- is somewhere between the extreme foremost and rearmost positions.
- The results of the damage value in the tube elements showed that this value reaches a maximum of 0.477, which is significantly lower than the critical value of 0.862; therefore, according to the Cockcroft-Latham failure criteria, no failure will occur.

## **Declarations**

Conflict of interest The authors declare that they have no conflict of interest.

## References

- Samipour S, Khaliulin V, Batrakov V (2018) Development of the technology of manufacturing Aerospace composite tubular elements by radial braiding. J Mach Manuf Reliab 47(3):284–289
- Syed A, Samal M, Chattopadhyay J, Dutta P (2020) Fracture toughness evaluation of axially-cracked tubular thin-walled specimens of Zircaloy-4 and its implications for integrity analysis of nuclear fuel clad. Theor Appl Fract Mech 106:102449
- Bortot P, Ceretti E, Giardini C (2008) The determination of flow stress of tubular material for hydroforming applications. J Mater Process Technol 203(1):381–388
- Zhang L, Xu W, Long J, Lei Z (2015) Surface roughening analysis of cold drawn tube based on macro–micro coupling finite element method. J Mater Process Technol 224:189–199
- Lee S-K, Jeong M-S, Kim B-M, Lee S-K, Lee S-B (2013) Die shape design of tube drawing process using FE analysis and optimization method. Int J Adv Manuf Technol 66(1–4):381–392
- Shaheen L (2007) Tube drawing principles: understanding processes, parameters key to quality. In: The tube and pipe journal.
  The tube & pipe association, International, pp 10–28
- Bramley A, Smith D (1976) Tube drawing with a floating plug. Metals Technology 3(1):322–331
- Łuksza J and Sadok L (1983) Wybrane zagadnienia z ciągarstwa AGH
- Gattmah J, Ozturk F, Orhan S (2020) A new development of measurement technique for residual stresses generated by the cold tube drawing process with a fixed mandrel. Int J Adv Manuf Technol 108(11):3675–3687
- Rubio E (2006) Analytical methods application to the study of tube drawing processes with fixed conical inner plug: slab and upper bound methods. J Achiev Mater Manuf Eng 14(1–2):119–130
- Świątkowski K, Hatalak R (2004) Study of the new floating-plug drawing process of thin-walled tubes. J Mater Process Technol 151(1–3):105–114

- Rubio EM, González C, Marcos M, Sebastián MA (2006) Energetic analysis of tube drawing processes with fixed plug by upper bound method. J Mater Process Technol 177(1):175–178
- Kwan C-T (2002) A generalized velocity field for axisymmetric tube drawing through an arbitrarily curved die with an arbitrarily curved plug. J Mater Process Technol 122(2–3):213–219
- Cockcroft M (1968) Ductility and workability of metals. J of Metals 96:2444
- Lee S, Ko D, Kim B, Lee J, Kim S, Lee Y (2007) A study on monobloc tube drawing for steering input shaft. J Mater Process Technol 191(1–3):55–58
- Rubio E, Camacho A, Pérez R, Marín M (2017) Guidelines for selecting plugs used in thin-walled tube drawing processes of metallic alloys. Metals 7(12):572
- Kuboki T, Nishida K, Sakaki T, Murata M (2008) Effect of plug on levelling of residual stress in tube drawing. J Mater Process Technol 204(1–3):162–168
- Haddi A, Imad A, Vega G (2011) Analysis of temperature and speed effects on the drawing stress for improving the wire drawing process. Mater Des 32(8):4310–4315
- Toribio J, Lorenzo M, Vergara D, Kharin V (2014) Influence of the die geometry on the hydrogen embrittlement susceptibility of cold drawn wires. Eng Fail Anal 36:215–225
- Chobaut N, Drezet J, Mischler S, Nguyen V, De Marco B, Dobler S, Rosset E (2019) Miniaturized tube fixed plug drawing: determination of the friction coefficients and drawing limit of 316 LVM stainless steel. J Mater Process Technol 263:396–407
- Cao TS (2017) Models for ductile damage and fracture prediction in cold bulk metal forming processes: a review. Int J Mater Form 10(2):139–171
- Kong Z, Zhang J, Li H, Kong N (2018) Deep drawing and bulging forming limit of dual-phase steel under different mechanical properties. Int J Adv Manuf Technol 97(5–8):2111–2124
- Farahani ND, Parvizi A, Barooni A, Naeini SA (2018) Optimum curved die profile for tube drawing process with fixed conical plug. Int J Adv Manuf Technol 97(1):1–11
- ASTMA53, (2020) Standard Specification for Pipe, Steel, Black and Hot-Dipped, Zinc-Coated, Welded and Seamless. ASTM International, West Conshohocken. PA
- Astm I, (2016) ASTM E8/E8M-16a: Standard Test Methods for Tension Testing of Metallic Materials. West Conshohocken, PA, USA: ASTM International
- Kim S, Kwon Y, Lee Y, Lee J (2007) Design of mandrel in tube drawing process for automotive steering input shaft. J Mater Process Technol 187:182–186
- Świątkowski K, Hatalak R (2006) Application of modified tools in the process of thin-walled tube drawing. Arch Metall Mater 51(2):193–197

**Publisher's Note** Springer Nature remains neutral with regard to jurisdictional claims in published maps and institutional affiliations.

